Optical and structural properties of silicon-rich silicon oxide films: Comparison of ion implantation and molecular beam deposition methods

Timur Nikitin*,1, Kerttu Aitola2, Sergei Novikov3, Markku Räsänen1, Rama Velagapudi4, Jani Sainio4, Jouko Lahtinen4, Kenichiro Mizohata5, Tommy Ahlgren5, and Leonid Khriachtchev,1**

1 Department of Chemistry, University of Helsinki, P. O. Box 55, 00014 Helsinki, Finland
2 Department of Applied Physics, Aalto University, P. O. Box 15100, 00076 Aalto, Finland
3 Electron Physics Laboratory, Aalto University, P. O. Box 3000, 02015 HUT Aalto, Finland
4 Department of Applied Physics, Aalto University, P. O. Box 11100, 00076 Aalto, Finland
5 Accelerator Laboratory, University of Helsinki, P. O. Box 43, 00014 Helsinki, Finland

* Corresponding author: e-mail timur.nikitin@helsinki.fi, Phone: +358 9 191 50278, Fax: +358 9 191 50279
** e-mail leonid.khriachtchev@helsinki.fi

We compare optical and structural properties of silicon-rich silicon oxide (SiO$_x$, $x \sim 1.8$) films obtained by ion implantation and molecular beam deposition (MBD). Before annealing, amorphous clusters (≥ 2 nm) are present in the MBD samples whereas these are absent for ion implantation, and the absorption at 488 nm is much stronger for MBD. Upon annealing, the absorption coefficient increases for the implanted material but the opposite change occurs for MBD. For both preparation methods, annealing at $\sim 1100\,°C$ produces silicon nanocrystals (Si-nc) and enhances the 1.5-eV photoluminescence (PL) whereas annealing at 1200 °C decreases the PL, especially for the implanted sample. The Si–SiO$_2$ phase separation is not complete even after annealing at 1200 °C.

© 2011 WILEY-VCH Verlag GmbH & Co. KGaA, Weinheim

1 Introduction Photonic applications of silicon nanostructures have been a challenging task since the discovery of bright photoluminescence (PL) from porous silicon [1]. Silicon-enriched silica is another material that can efficiently emit light [2]. The PL at ~ 1.5 eV has been attributed to quantum confinement in silicon nanocrystals (Si-nc) [3–5], light-emitting centers at the Si/SiO$_2$ interface [6–9], or oxygen-related defects in more disordered silicon-rich areas [10, 11]. The light-emitting centers have been suggested to contain non-bridging oxygen (Si=O) [12]. Si-nc in silica can be produced by annealing of silicon-rich silicon oxide SiO$_x$ ($x < 2$) prepared by plasma enhanced chemical vapor deposition (PECVD) [9, 13–15], magnetron sputtering [13, 14], molecular beam deposition (MBD) [10, 11, 16, 17], and Si-ion implantation [4, 18]. The optical and structural properties of SiO$_x$ films prepared by PECVD and magnetron sputtering have recently been compared [13, 14]. Such

systematic analysis is important since it is generally difficult to compare reports on SiO$_x$ samples prepared by different methods and treated under different conditions. In the present work, we apply Raman, PL, and UV–visible transmission spectroscopies, X-ray photoelectron spectroscopy (XPS), and time-of-flight elastic recoil detection analysis (ToF-ERDA) to compare optical and structural properties of SiO$_x$ films fabricated by MBD and ion implantation, which are perspective methods for preparation of Si-based photonic materials [2].

2 Experimental details The implantation of Si ions into a silica plate was done with six different energies (30, 56, 98, 160, 250, and 400 keV) and doses by a high voltage engineering implanter to achieve a nearly constant Si excess in the layer with a thickness of ~ 750 nm. This sample was annealed at various temperatures up to 1200 °C for 1 h in

Phys. Status Solidi A **208**, No. 9 (2011)

2177

nitrogen atmosphere and studied after each annealing step. The MBD SiO$_x$ films with varied Si concentration were deposited onto a silica substrate and annealed from 400 (as-prepared sample) to 1200 °C [10, 16, 17].

The O/Si concentration ratios were estimated by ToF-ERDA and XPS. For the implanted sample, both methods yielded $x \sim 1.8$ (Si excess ~ 3.6 at.%, total Si content ~ 36 at.%). Two areas (A and B) with slightly different Si excess were studied in detail for the MBD samples. For area A, the XPS method yielded $x \sim 1.7$ and ToF-ERDA gave $x \sim 1.6$. For area B, both methods yielded $x \sim 1.8$. The PL and Raman signals from these two MBD areas differ by 12–23% after annealing at 1100–1200 °C, which estimates the uncertainty in area selection and the experimental error.

The thickness d of the MBD film was 1860 and 1600 nm for areas A and B, respectively, as estimated using the PL filtering effect [16, 17, 19]. The absorption coefficients at 488 nm, α, were obtained from the transmission and reflection spectra, recorded with a fiber-optics spectrometer (SD2000, Ocean Optics), and a broadband light source (DH-2000, Top Sensor Systems) [20]. The PL and Raman spectra were measured with an argon ion laser (488 nm, Omnichrome 543-AP), a spectrometer (Acton SpectraPro 500I), and a charge-coupled device camera (Andor InstaSpec IV). The Raman and PL intensities were normalized by the effective thickness:

$$\int_0^d e^{(-2\alpha x)} dx \quad \text{and} \quad \int_0^d e^{(-\alpha x)} dx,$$

respectively, assuming the same absorption coefficients for the laser and Raman light and neglecting the absorption for the PL at ~ 800 nm [21].

The XPS measurements were done with a SSX-100 instrument using monochromated Al Kα radiation, and the samples were sputtered with 4 keV Ar ions to obtain the composition as a function of depth. The Si 2p XPS spectra were fitted by three Gaussians providing the proportion of Si bonded as in bulk Si (elemental Si), "SiO" (mixture of various suboxides), and SiO$_2$ materials [16, 17]. The ToF-ERDA equipment and procedures are described elsewhere [22].

3 Results When annealed below 900 °C, both types of samples show a PL with a maximum at about 650–700 nm, which is substantially stronger for the implanted sample (Fig. 1a). Annealing at 1100–1150 °C red-shifts the PL to ~ 800 nm (Fig. 1b) and strongly increases the PL intensity (Fig. 1c), the normalized PL being slightly stronger for the implanted sample. Annealing at 1200 °C further red-shifts the PL but decreases the PL intensity, and these changes are much more pronounced for the implanted sample.

The Raman spectra and absorption are quite different for the as-prepared samples. The MBD samples annealed up to ~ 900 °C display a broad Raman band at ~ 470 cm^{-1} (Fig. 2a), and the absorption coefficient at 488 nm is
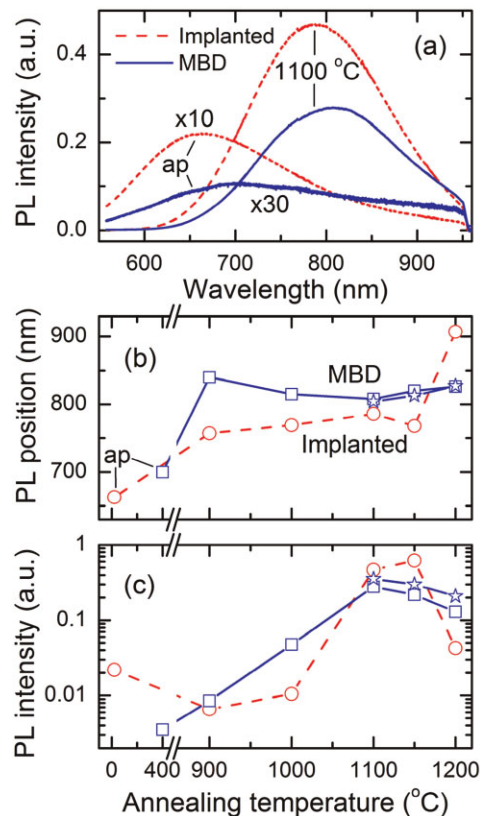
Figure 1 (online color at: www.pss-a.com) (a) PL spectra of as-prepared (ap) and annealed at 1100 °C SiO$_x$ films fabricated by MBD (area A) and ion implantation. (b) PL position and (c) normalized PL intensity for MBD (squares for area A and stars for area B) and implanted sample (circles) as a function of the annealing temperature.

relatively large ($\sim 10^4$ cm^{-1}) (Fig. 2d). In contrast, no Raman band is observed for the implanted sample (Fig. 2b), and the absorption coefficient is quite small (~ 300 cm^{-1}) (Fig. 2d). A narrow Raman band at 516–517 cm^{-1} emerges after annealing above 1000 °C featuring the formation of Si-nc in both types of samples. The low frequency shoulder at 490–500 cm^{-1} of the Raman band is observed due to residual disordered Si phase or small Si clusters (<2 nm) [16, 23]. The Raman spectra were fitted with two Lorentzians [16]. The Raman shift for the higher-frequency component (ordered phase) tends to increase as the annealing temperature increases from 1000 to 1200 °C (Fig. 2c). For the MBD samples, the absorption is the highest after deposition and it decreases with the increasing annealing temperature (Fig. 2d). In contrast, for the implanted sample, the absorption increases for annealing above 800 °C. The absorption coefficients of $\sim 10^3$ cm^{-1} obtained for both types of samples after annealing at 1100–1200 °C agree with the previous report on similar SiO$_x$ materials [16].

For all samples, the XPS spectra indicate only a few percent of elemental Si, 15–20% of Si in suboxides, and $\sim 80\%$ of Si in SiO$_2$. The amount of elemental Si tends to
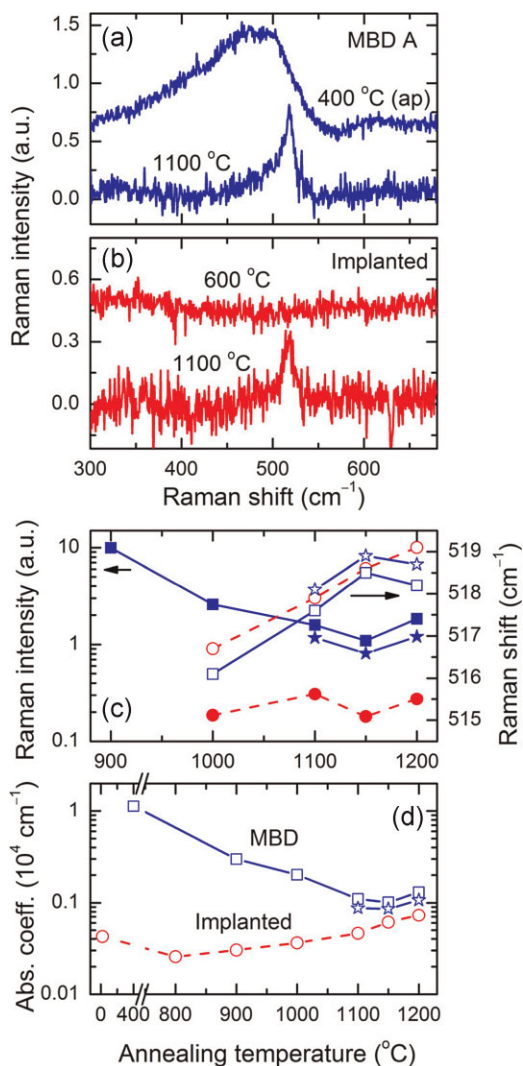
Figure 2 (online color at: www.pss-a.com) Raman spectra of SiO_x films prepared by (a) MBD (area A) and (b) ion implantation and annealed at different temperatures. The spectra are vertically shifted for better presentation. (c) Normalized intensity (solid symbols) and position of the maximum (open symbols) of the Raman band, and (d) absorption coefficient at 488 nm as a function of the annealing temperature. The symbols are the same as in Fig. 1.

increase for higher annealing temperatures, being somewhat smaller in the implanted sample. For both types of samples, no correlation between the PL intensity and the amount of Si in elemental Si or oxidation states was found at different annealing stages.

We also estimated the band gap using the Tauc relation [4, 14, 24]. For the MBD samples, the band gap is ~2.2, 2.4, and 2.6 eV after annealing at 900, 1000, and 1100–1200 °C, respectively. For the implanted sample it is ~3.3 and 2.8 eV after annealing at 1150 and 1200 °C, respectively.

4 Discussion
4.1 Structural properties
First, we compare structural properties of the SiO_x samples for the two deposition

methods. For MBD, relatively large amorphous Si inclusions are observed after deposition ($\geq$2–3 nm), as suggested by the presence of the broad Raman band at ~470 cm^{-1} [21, 25] and high absorption. Indeed, a study of Si/SiO_2 superlattices has revealed that the Raman bands of amorphous Si are observed for thicker Si layers ($\geq$2 nm) and the Raman-scattering cross-section decreases for thinner Si layers correlating with decreasing absorption [21]. Annealing at higher temperatures ($\geq$1000 °C) results in ordering (crystallization) of the amorphous Si inclusions as evidenced by the narrowing and upshift of the Raman band from ~470 to ~516 cm^{-1}. As a result of annealing, the absorption coefficient decreases, which is reasonable because absorption is much smaller for crystalline silicon than for amorphous silicon. Similarly, the absorption coefficient decreased for Si/SiO_2 superlattices with amorphous Si layers with thickness >2 nm after annealing at 1000 °C [21]. On the other hand, the Si grain sizes in the MBD samples do not probably increase substantially after annealing, since the band gap does not decrease. A small increase of the Si-nc sizes is probable after annealing at 1200 °C, since the PL slightly red-shifts and the absorption coefficient and Raman intensity increase.

For the implanted sample annealed up to 900 °C, only very small Si clusters (with sizes up to ~1 nm) may be present, as suggested by the absence of Raman bands and very low absorption [21]. The Raman intensity and the absorption coefficient increase upon annealing above 1000 °C. An increase of absorption was observed for thin amorphous Si layers (0.8 and 1.2 nm) in Si/SiO_2 superlattices after annealing at 1000 °C [21], which was explained by an increase of absorbing Si phase in the material. Based on the Raman and absorption measurements, we conclude that the Si clusters grow and crystallize in the implanted sample upon annealing above 1000 °C, which has previously been validated by TEM for implanted [18] and PECVD [15] samples. Annealing at 1200 °C increases the Si-nc sizes in the implanted sample, which is suggested by the decrease of the band gap, increase of the absorption coefficient and normalized Raman intensity. In accord, the Raman band up-shifts after annealing at 1200 °C (Fig. 2c); however, the position of Si-nc band can be affected by tensile stress of the Si-nc [10, 16], although this contribution to the temperature dependence should be minor.

The higher absorption and normalized Raman intensity are observed after annealing for the MBD samples compared to the implanted sample, suggesting that the amount of Si-nc with sizes $\geq$2 nm is greater in the MBD samples. The absorption coefficient correlates with the integrated Raman intensity at all annealing temperatures, which is in agreement with the previous results [10]. The smaller average band gap for the MBD samples annealed at 1150 °C (~2.6 eV) compared to that for the implanted sample (~3.3 eV) also indicates the larger average Si-nc sizes for the MBD samples.

The quantitative estimates of Si-nc sizes should be considered with caution. After annealing above 1100 °C, the typical Si-nc sizes of 3–4 nm were estimated from Raman

Phys. Status Solidi A **208**, No. 9 (2011)

Original

Paper

2179

spectra [10] using the phonon confinement model [23, 26] and found by TEM for SiO_x materials [15, 18, 27]. The band gaps obtained in the present work ($\sim$3 eV) are usually connected to absorption of Si grains with diameters of 1–2 nm [18]. Such small Si grains are at the detection edge by Raman spectroscopy and correspond to the band shoulder at 490–500 cm^{-1} in Raman spectra [16, 23]. Large Si-nc (i.e., 3–4 nm) presumably possess larger Raman-scattering cross-section and therefore contribute more to the Raman spectrum. On the other hand, very small Si clusters with sizes $\sim$1 nm and below, are not detectable by TEM and Raman spectroscopy; thus, their proportion is difficult to estimate. This explains the seeming disagreement between the Si-nc sizes obtained from the phonon confinement model and absorption measurements. It should also be mentioned that the band gap of Si clusters is a complex function of a number of parameters in addition to the size, such as the crystallinity, strain due to the silica matrix, and interface passivation [28–30]. Moreover, the Tauc law is generally applicable for amorphous semiconductors with absorption coefficients $>10^4$ cm^{-1} [24]. Therefore, the band gaps obtained in the present work by applying the Tauc law to crystalline Si grains may be inaccurate, and hence lead to only rough estimation of Si-nc sizes. Nevertheless, this approach has previously been used for Si-nc yielding reasonable results [4, 14]. For SiO_x films prepared by PECVD and magnetron sputtering, Mirabella et al. [14] reported an increase of the band gap from 2.2 to 2.6 eV with the annealing temperature, which is in good agreement with the present data for the MBD samples. This increase of the band gap was explained by amorphous-to-crystalline transitions of the Si clusters at high annealing temperatures rather than by a decrease of their sizes. Garrido Fernandez et al. [18] obtained somewhat smaller band gap by utilizing the PL excitation method. Thus, the Si-nc sizes estimated from both Raman spectra and absorption measurements should be considered rather qualitatively than quantitatively.

The suboxide component is clearly present in the XPS spectra (15–20%) and the elemental Si component is small for both types of samples annealed at 1200 °C. This shows that the Si–SiO_2 phase separation is not complete after annealing at 1200 °C, in agreement with the earlier results [16, 17], and Si-nc consume a minor part of the Si excess. Similarly, it has been reported that a major part of the Si excess in PECVD samples is either embedded in clusters too small to be detected by TEM and EFTEM or is still dissolved in the SiO_x matrix [13–15]. A more quantitative analysis of the proportion of Si in elemental Si, "SiO," and SiO_2 is difficult due to fitting uncertainties of XPS spectra for SiO_x films with such low Si excess. A complete phase separation has recently been achieved by laser annealing of SiO_x free-standing films at temperatures above 1400 °C [31].

4.2 Light-emitting properties The PL at $\sim$660 nm from the as-prepared implanted sample can be ascribed to various radiative defects, for instance, non-bridging oxygen–hole centers or E'-type defects [4, 18]. The amount of these

defects is obviously smaller in the MBD samples since the PL from the MBD samples is much weaker compared to that from the implanted sample. After annealing at 900 °C, the PL intensity of the implanted sample decreases indicating that these initial defects are thermodynamically unstable, and hence they decompose.

The 1.5-eV PL intensity rises upon annealing above 1000 °C for both types of samples. Non-radiative defects such as dangling bonds at the Si-nc/SiO_2 interface as well as defects inside and outside the Si-nc can efficiently trap the excitation and therefore quench the PL [12, 32, 33]. Annealing at $\sim$1100 °C presumably decreases the amount of these non-radiative defects and/or intensifies an energy transfer to radiative centers, which enhances the PL. The amount of the light-emitting centers may increase upon annealing, however, no direct evidence of this is available.

The mechanism of the red PL is still a subject to debate. The defect origin has recently been confirmed by Godefroo et al. [32] for similar materials. The light-emitting centers, probably containing oxygen, may be located at the Si/SiO_2 interface of Si-nc [6–9, 12] and/or in disordered silicon-rich areas [10, 11]. The light-emitting centers can be excited directly or the excitation can migrate to them from the absorbing Si phase [11]. This model is in line with the absence of correlation between the PL intensity and the amount of elemental Si or suboxides at different annealing stages. After annealing at 1100–1150 °C the normalized PL intensity is higher for the implanted sample despite the smaller amount of elemental Si, which is consistent with the "defect" origin of the PL. In addition to lattice defects, the PL can originate from very small Si grains. Theoretical calculations by Guerra and Ossicini [34] have recently suggested that the most optically active Si/SiO_2 structures could be the smallest (0.2–1.5 nm), highly oxidized, crystalline Si grains. In agreement, it was found that the PL quantum yield increases with the decrease of the proportion of elemental Si and large Si-nc ($\sim$3–4 nm) are not required for this PL [11]. The very small Si grains, however, cannot be directly monitored by Raman spectroscopy due to their very low Raman scattering cross-section and by TEM. Moreover, the very small and strongly oxidized Si grains may be difficult to discriminate from suboxides by XPS measurements of the binding energies. The XPS results on elemental Si are probably connected with rather large Si grains that are visible in Raman spectra [17].

After annealing at 1100–1200 °C, the energies of the PL are smaller than the obtained band gaps by about 1 and 1.5 eV for the MBD and implanted samples, respectively. These values for the Stokes shift are comparable to those presented by Mirabella et al. [14] but quite larger than a value of $\sim$0.26 eV obtained by Garrido Fernandez et al. [18]. Wolkin et al. [12] also observed large Stokes shifts for the smallest nanocrystallites ($<$1.5 nm) and explained it by trapping of the excitation by the Si=O bonds. In addition to trapping by surface states [35], the high Stokes shifts could be due to energy losses when the excitation migrates from absorbing Si grains to light-emitting centers located in disordered

areas [11] that can be the optically active small Si-nc grains [34]. Direct excitation of the small Si grains is also possible. The calculated band gaps of these Si clusters (diameters ~1 nm) are 2–3 eV [34], which is comparable to those obtained in the present work.

The decrease of the PL intensity by annealing at 1200 °C is consistent with the origin of the PL from small light-emitting centers, if these centers can decompose at such high temperatures. As an example, the Si=O bonds, suggested by Wolkin et al. [12] as a possible light-emitting center, are less stable than the O–Si–O structures. The PL intensity can also decrease if the amount of small optically active Si/SiO$_2$ nanocrystals considered by Guerra and Ossicini [34] decreases at this temperature. The red-shift of the PL by annealing at 1200 °C can originate from a thermal modification of the light-emitting centers, for example, an increase of the size of oxidized small Si grains [34]. In terms of energy transfer from the absorbing to the emitting phase [11], the PL energy is connected with the band gap of the absorbing phase, which would lead to the same trend.

5 Conclusions The structural and optical properties of SiO$_x$ materials with similar Si excess prepared by MBD and ion implantation are very different for as-prepared samples but become similar after annealing above 1000 °C. After fabrication, the MBD sample contains relatively large amorphous Si inclusions ($\geq$2 nm) and shows a large absorption coefficient at 488 nm, whereas these are absent in the implanted sample and the material is optically transparent. Annealing above 1000 °C leads to the crystallization of the amorphous Si grains in the MBD samples and to the growth and crystallization of Si clusters in the implanted sample. After annealing, the absorption coefficient generally decreases for the MBD sample and increases for the implanted sample, in agreement with the structural modifications in these materials.

After annealing above 1000 °C, the enhancement of the 1.5-eV PL intensity for both preparation methods can be explained by thermal passivation of non-radiative defects and/or due to formation of light-emitting centers such as oxygen-related defects or small highly oxidized crystalline Si grains [34]. The PL decreases and shifts to red after annealing at 1200 °C probably due to a combination of several reasons, for example, modification of the light-emitting centers. The detailed mechanisms of the PL in these materials are still not well understood.

The Si/SiO$_2$ phase separation is not complete even after annealing at 1200 °C, and a large proportion of suboxides is still present in the materials according to the XPS measurements. The proportion of very small Si-nc (<1 nm) is difficult to discuss because they are practically undetectable by the available analytical methods. On the other hand, the optical and light-emitting properties of Si-rich silicon oxide can be essentially contributed by such ultra-small grains [34].

References

[1] L. T. Canham, Appl. Phys. Lett. **57**, 1046 (1990).
[2] L. Khriachtchev, (ed.), Silicon Nanophotonics: Basic Principles, Present Status and Perspectives (Pan Stanford, Singapore, 2008).
[3] P. Mutti, G. Ghislotti, S. Bertoni, L. Bonoldi, G. F. Cerofolini, L. Meda, E. Grilli, and M. Guzzi, Appl. Phys. Lett. **66**, 851 (1995).
[4] S. Guha, J. Appl. Phys. **84**, 5210 (1998).
[5] G. Ledoux, J. Gong, F. Huisken, O. Guillois, and C. Reynaud, Appl. Phys. Lett. **80**, 4834 (2002).
[6] Y. Kanemitsu, T. Ogawa, K. Shiraishi, and K. Takeda, Phys. Rev. B **48**, 4883 (1993).
[7] S. Prokes, Appl. Phys. Lett. **62**, 3244 (1993).
[8] J. L. Gole, F. P. Dudel, D. Grantier, and D. A. Dixon, Phys. Rev. B **56**, 2137 (1997).
[9] N. Daldosso, M. Luppi, S. Ossicini, E. Degoli, R. Magri, G. Dalba, P. Fornasini, R. Grisenti, F. Rocca, L. Pavesi, S. Boninelli, F. Priolo, C. Spinella, and F. Iacona, Phys. Rev. B **68**, 085327 (2003).
[10] L. Khriachtchev, M. Räsänen, S. Novikov, and L. Pavesi, Appl. Phys. Lett. **85**, 1511 (2004).
[11] L. Khriachtchev, T. Nikitin, R. Velagapudi, J. Lahtinen, and S. Novikov, Appl. Phys. Lett. **94**, 043115 (2009).
[12] M. V. Wolkin, J. Jorne, P. M. Fauchet, G. Allan, and C. Delerue, Phys. Rev. Lett. **82**, 197 (1999).
[13] G. Franzò, M. Miritello, S. Boninelli, R. Lo Savio, M. G. Grimaldi, F. Priolo, F. Iacona, G. Nicotra, C. Spinella, and S. Coffa, J. Appl. Phys. **104**, 094306 (2008).
[14] S. Mirabella, R. Agosta, G. Franzò, I. Crupi, M. Miritello, R. Lo Savio, M. A. Di Stefano, S. Di Marco, F. Simone, and A. Terrasi, J. Appl. Phys. **106**, 103505 (2009).
[15] S. Boninelli, F. Iacona, G. Franzò, C. Bongiorno, C. Spinella, and F. Priolo, J. Phys.: Condens. Matter **19**, 225003 (2007).
[16] L. Khriachtchev, M. Räsänen, S. Novikov, and J. Lahtinen, J. Appl. Phys. **95**, 7592 (2004).
[17] L. Khriachtchev, T. Nikitin, C. J. Oton, R. Velagapudi, J. Sainio, J. Lahtinen, and S. Novikov, J. Appl. Phys. **104**, 104316 (2008).
[18] B. Garrido Fernandez, M. López, C. Garcia, A. Pérez-Rodríguez, J. R. Morante, C. Bonafos, M. Carrada, and A. Claverie, J. Appl. Phys. **91**, 798 (2002).
[19] L. Khriachtchev, M. Räsänen, and S. Novikov, Appl. Phys. Lett. **83**, 3018 (2003).
[20] L. Khriachtchev, Appl. Phys. Lett. **81**, 1357 (2002).
[21] L. Khriachtchev, M. Räsänen, S. Novikov, O. Kilpelä, and J. Sinkkonen, J. Appl. Phys. **86**, 5601 (1999).
[22] J. Jokinen, J. Keinonen, P. Tikkanen, A. Kuronen, T. Ahlgren, and K. Nordlund, Nucl. Instrum. Methods B **119**, 533–542 (1996).
[23] G. Faraci, S. Gibilisco, P. Russo, A. R. Pennisi, and S. La Rosa, Phys. Rev. B **73**, 033307 (2006).
[24] S. Knief and W. von Niessen, Phys. Rev. B **59**, 12940 (1999).
[25] A. Hartstein, J. C. Tsang, D. J. DiMaria, and D. W. Dong, Appl. Phys. Lett. **36**, 836 (1980).
[26] J. H. Campbell and P. M. Fauchet, Solid State Commun. **58**, 739 (1986).

Original

Paper

Phys. Status Solidi A **208**, No. 9 (2011)

2181

[27] S. Novikov, J. Sinkkonen, T. Nikitin, L. Khriachtchev, M. Räsänen, and E. Haimi, Microelectron. J. **39**, 518 (2008).

[28] L. Koponen, L. O. Tunturivuori, M. J. Puska, and R. M. Nieminen, Phys. Rev. B **79**, 235332 (2009).

[29] R. Guerra, I. Marri, R. Magri, L. Martin-Samos, O. Pulci, E. Degoli, and S. Ossicini, Phys. Rev. B **79**, 155320 (2009).

[30] R. Guerra, E. Degoli, and S. Ossicini, Phys. Rev. B **80**, 155332 (2009).

[31] L. Khriachtchev, T. Nikitin, M. Räsänen, A. Domanskaya, S. Boninelli, F. Iacona, A. Engdahl, J. Juhanoja, and S. Novikov, J. Appl. Phys. **108**, 124301 (2010).

[32] S. Godefroo, M. Hayne, M. Jivanescu, A. Stesmans, M. Zacharias, O. I. Lebedev, G. Van Tendeloo, and V. V. Moshchalkov, Nat. Nanotechnol. **3**, 174 (2008).

[33] D. Hiller, M. Jivanescu, A. Stesmans, and M. Zacharias, J. Appl. Phys. **107**, 084309 (2010).

[34] R. Guerra and S. Ossicini, Phys. Rev. B **81**, 245307 (2010).

[35] F. Koch, V. Petrova-Koch, and T. Muschik, J. Lumin. **57**, 271 (1993).